PFC/JA-96-33

Radiative and 3-Body Recombination in Alcator C-Mod

D. Lumma, J.L. Terry, B. Lipschultz

October 1996

Submitted to Physics of Plasmas.

This work was supported by the U. S. Department of Energy Contract No. DE-AC02-78ET51013. Reproduction, translation, publication, use and disposal, in whole or in part by or for the United States government is permitted.

Radiative and 3-body recombination in the Alcator C-Mod divertor

D. Lumma, J.L. Terry, and B. Lipschultz
Plasma Fusion Center, Massachusetts Institute of Technology
Cambridge, MA 02139, U.S.A.

Significant recombination of the majority ion species has been observed in the divertor region of Alcator C-Mod under detached conditions. This determination is made by analysis of the visible spectrum from the divertor, in particular the Balmer series line emission and the observed recombination continuum, including an apparent recombination edge at ~375 nm. The analysis shows that the electron temperature in the recombining plasma is 0.8-1.5 eV. The measured volume recombination rate is comparable to the rate of ion collection at the divertor plates. The dominant recombination mechanism is 3-body recombination into excited states ($e+e+D^+ \Rightarrow D_0+e$), although radiative recombination ($e+D^+ \Rightarrow D_0+h\nu$) contributes ~5% to the total rate. Analysis of the Balmer series line intensities (from n_{upper}=3 through 10) shows that the upper levels of these transitions are populated primarily by recombination. Thus the brightnesses of the Balmer series (and Lyman series) are directly related to the recombination rate.

(PACS numbers 34.50.Dy, 34.80.Lx, 52.25.Ya, 52.55.Fa)

I. Introduction

Utilization of atomic processes in the dispersal of plasma heat flow before reaching the divertor plates is a focus of current divertor plasma research. This is required because of the enormous parallel flows in a reactor that in steady state are beyond present materials' capabilities. The required volumetric losses are expected to be dominated by line radiation. Charge-exchange between hydrogenic ions and neutrals has been shown theoretically to be important in removing ion momentum.[1] Removal of momentum permits higher radiation (line) losses.[2] The role of charge-exchange in energy removal is less clear from experiments but is still likely to be significant.[3]

Recombination, until recently, was theoretically discounted with respect to energy or momentum removal. However, low-T_e measurements from the divertor plasmas found in Alcator C-Mod[4] and DIII-D,[5] as well as the inability to explain divertor ion current loss during detachment[6,7] have returned attention to recombination and to its role in divertor physics. In particular, it is important to determine its role in divertor detachment.[1,8]

Several variations of recombination can lead to the conversion of hydrogenic ions into ground state neutral atoms. These include 3-body recombination ($e+e+D^+ \Rightarrow D_0+e$), radiative (2-body) recombination ($e+D^+ \Rightarrow D_0+h\nu$) or various paths through excited hydrogenic molecules (e.g. $D_2^+ + e \Rightarrow 2D$).[9-11] All of the above processes may be important in the temperature range 1-3 eV.

It is important to define what we mean by recombination. In any hydrogenic plasma there is an atomic level n*, above which the population densities of bound and free electrons are effectively in Saha-Boltzmann equilibrium. This level is also called the "collision limit",[12] since the populations are determined overwhelmingly by collisions (mainly 3-body recombination and its inverse, electron impact ionization). Those atoms whose bound states are above this limit do not remove energy and momentum from the divertor plasma, since they are so quickly re-ionized. In comparison, a ground state atom is relatively long lived.

We use the term 'recombination' to denote the general process of conversion of an ion and free electron into a neutral, typically an excited neutral. However, we will designate as 'complete' recombinations those recombinations which result in neutrals in the ground state. This is the same sense in which the recombination rate coefficients are calculated.[10,13] It is impor-

tant to note that recombination from the continuum into excited neutral hydrogenic states occurs constantly. This is quickly followed, in most cases, by ionization back to the continuum, and thus does not result in the conversion of an ion to a neutral in the ground state, that is, in a 'complete' recombination.

In this paper we demonstrate methods developed to determine the amount and kind of recombination occurring in plasmas. We also present the first direct experimental measurement of significant recombination of the majority ion species in the divertor region of a tokamak. However, this paper is not a general exposition on the scalings and characteristics of recombination in divertor plasmas.

The work described here is primarily an analysis of the visible spectrum emitted from the divertor plasma. In particular, three analyses are performed on the spectrum: (1) The continuum emission is used to determine the radiative - 2-body - recombination rate directly into the ground state, Ψ_{2bdy}, as well as the local electron temperature of the emitting region (section IV). (2) The Stark broadening of the Balmer series lines is used to determine the local density in the emitting region (section III). (3) The Balmer series intensities are used to determine the rate of 'complete' recombinations which are preceded by recombination into excited neutral states and which decay radiatively to the ground state, $\Psi_{n>0}$ (section V). These recombinations have a 'signature' photon resulting from the subsequent decay to the ground state. $\Psi_{n>0}$ is dominated by 3-body recombination.

Finally, a total rate of 'complete' recombinations, Ψ_{rec}, is determined and compared with the magnitude of the other sink for ions (section VI). The rate of 'complete' 3-body recombinations which have reached the ground state by collisional de-excitation, $\Psi_{photonless}$, is calculated based on the above information through the relationship: $\Psi_{rec} = \Psi_{n>0} + \Psi_{2bdy} + \Psi_{photonless}$. Of course, those recombinations accounted for by $\Psi_{photonless}$ have no 'signature' photons associated with them. The relative magnitudes of these three processes are $\Psi_{n>0} : \Psi_{2bdy} : \Psi_{photonless} \approx 90 : 5 : 5$.

II. The Experiment

Alcator C-Mod is a high-field tokamak which normally operates with a single-null divertor located at the bottom of the machine with $\vec{B} \times \nabla B$ towards the divertor. The divertor geometry is such that most of the divertor plate surfaces are almost vertical, a design now incorporated for ITER.[14] The combination of high-field and vertical plate geometry leads to a capability of operating both the divertor and core plasmas at very high density ($N_{e,div} \geq 1 \cdot 10^{21}\,m^{-3}$). A description of the general machine operation can be found elsewhere.[15]

For the presentation of the analysis technique described in this paper, we have used a series of similar shots. The main plasma parameters are given by plasma current of 800 kA, $\overline{n}_e = 2.1 \cdot 10^{20}\,m^{-3}$, $P_{ICRF} = 1.40\,MW$ and L-mode energy confinement. At this main plasma density, the divertor plasma was in a detached state, characterized by a large drop in plasma pressure near the plates and very low electron temperatures at the plates.[4]

The primary diagnostic used for this study is a multiple-view spectrometer system. The spectrograph has a focal length of 250 mm and an aperture ratio of $f/4$. A two-dimensional CCD detector is mounted at the exit plane of the instrument. Visible and UV emission carried by up to 14 fibers, stacked vertically at the entrance slit, is imaged vertically at the exit plane and spectrally dispersed in the horizontal direction. There are 1242 spectral pixels and 14 spatial bins. The spatial bins are groups of physical pixels, summed during the readout cycle. This binning allows a reduction in the readout time of the entire CCD. Employing a grating blazed at 250 nm with 1800 grooves per mm, the nominal spectral resolution is $\sim$ 0.8 Å. For these experiments one of the quartz fibers at the entrance slit viewed the plasma and, more importantly, the closed C-Mod divertor region, through a re-entrant quartz window. This field of view is shown in Fig. 1a.

Additionally, the same poloidal region of the plasma is imaged onto a linear array of 64 silicon diodes through a D_α interference filter ($\lambda_0 = 657$ nm, $\Delta\lambda_{FWHM} = 5.6\,nm$).[16] The 64 chords, which are displaced toroidally from the spectrograph view, result in a spatial resolution of about 2 cm in a horizontal plane in the divertor. A typical brightness profile for D_α from the diode array is shown in Fig. 1b. Additional diode arrays, also filtered at D_α, view the plasma from different angles. Tomographic inversions of the brightness data result in emissivity profiles showing that almost all the D_α

emission comes from the divertor region and is within the field of view of the spectrograph.[17,16]

The intensity calibration of the entire optical system of the spectrograph and of the D_α array was achieved using an absolute source, model US-060-SF produced by Labsphere, Inc. It is a 45 Watt halogen lamp illuminating the inside of a sphere with a circular opening and with a spatially uniform output radiance. The spectral radiance curve of the lamp is known for wavelengths between 300 nm and 2400 nm. We estimate the intensity calibration of the spectrograph system to be accurate to within approximately $\pm 15\%$. Accounting for the spectrograph's field-of-view and time resolution, the sensitivity calibration of the filtered array was checked against that of the spectrograph by measuring the D_α brightnesses on the same shot. The brightnesses agree to within $\pm 10\%$, thus legitimizing the inclusion in the analyses of the array D_α brightnesses with other Balmer series line brightnesses measured by the spectrometer. The wavelength calibration of the spectrograph is based on measurements of hydrogen and mercury emission lines from low-pressure and low-temperature laboratory lamps.

III. Presentation of Spectrum

The measured spectrum at the Balmer series limit and around the recombination 'edge', indicative of recombination into $n = 2$, is shown in Fig. 2. A number of general features are evident in this spectrum:

- Comparison of the underlying continuum emission at wavelengths $\lesssim$ 370 nm with that at wavelengths $\gtrsim$ 400 nm shows a clear change in the continuum brightness.
- The Balmer series lines from $n = 5 \rightarrow n' = 2$ to $n = 11 \rightarrow n' = 2$ are resolved.
- These lines are broadened relative to the other lines in the spectrum which arise from plasma impurities.

The magnitude of the 'edge' in the continuum radiation will be used to determine the electron temperature in the region of emission (section IV). The intensities of the Balmer spectrum will be used to determine how dominant recombination is in relation to excitation and the total rate of 'complete' recombinations (section V).

A. Stark Broadening

The Balmer lines visible in the spectrum are strongly Stark broadened, which indicates a high electron density in the region of emission. This effect has been used to determine the electron density in the region of Balmer line emission.[18,19] The theoretical framework and the numerical details of this analysis are described elsewhere.[19] This procedure yields an electron density, at the time the spectrum shown in Fig. 2 was measured, of approximately $N_e = 8.8 \cdot 10^{20}\,\mathrm{m}^{-3}$ with an uncertainty of about $\pm 20\%$.

As a result of this high electron density, we do not observe the step in the continuum emission, the recombination 'edge', at the wavelength corresponding to the ionization limit ($n = 2$) of an *isolated* neutral atom ($\lambda_\infty = 364.5\,\mathrm{nm}$). What is observed instead is a gradual merging of the Balmer series lines into a continuum. This is a combination of two effects: bound states merging into one another (Stark broadening) and the conversion of bound states into continuum brought about by the presence of the plasma electrons in the atoms' near environment. Inglis and Teller have dealt

with the former.[20] That formalism relates the local density to the highest energy transition which can be resolved. Using the density obtained from the Stark broadening analysis of the resolved lines, the Inglis-Teller formalism predicts that lines up to $n = 13$ should be resolved, whereas, experimentally only lines up to $n = 11$ are resolved. At present we do not understand the reason for this difference. It is the object of further study.

IV. Analysis of the Continuum Radiation

There are three physical sources contributing to the overall continuum spectrum emitted within the field of view:

- Bremsstrahlung originating in the hot core of the plasma body due to deuterium and impurities.
- Bremsstrahlung originating in the divertor.
- Radiative 2-body recombination occurring in the divertor.

Calculation of the bremsstrahlung contribution from the core (section IV.B) requires knowledge of the profiles for core electron temperature and core electron density as well as Z_{eff}. We model the divertor emission as coming from an isothermal, uniform-density plasma. The emitting volume is assumed to be an annular disk of average thickness, ΔL, perpendicular to the central ray of the view, and the emission is assumed to be toroidally axisymmetric. The radial edges of the emitting divertor volume are defined by the intersection of the spectrometer field of view with the inner and outer divertor plates (Fig. 1a). For reference we call this the 'divertor emission region'. Its volume is $A_v \, \Delta L$, where $A_v \approx 0.72\,\mathrm{m}^2$. Of course, in reality, conditions are not uniform within this volume, and the shape of the actual emitting volume is much more complicated. The effect of these assumptions is examined in section VI.

From the spatially resolved measurements of the D_α brightness, shown in Fig. 1(b), it is seen that there is some spatial variation in brightness, with brightness maxima along chords striking near the inner 'nose' of the divertor and along chords through the X-pt region. However, the spectrometer view, having no spatial resolution, measures only the average brightness from within its field-of-view. This spatially averaged spectrum reveals a dominant

temperature and density which give rise to the emission. The assumptions about the geometric structure of the emitting volume allow us to relate the measured brightness to the calculated emissivities and to calculate the projected surface area of the volume so that *total* 'complete' recombination rates can be determined. In the calculations, the plasma in the 'divertor emission region' has an ion density N_i and an electron density N_e, where the ions are assumed to carry a charge of $+Ze$. The ions are assumed to exhibit no thermal motion, whereas the random electron motion will be described by an underlying Maxwellian velocity distribution characterized by a temperature T_e.

A. General Equation

The hydrogenic plasma described above will emit a continuum radiation due to the combined effects of radiative recombination and bremsstrahlung. The emissivity corresponding to these processes are[21]:

$$\begin{aligned} \frac{W_\nu(T_e,\nu)}{4\pi}d\nu &= \frac{W_{\nu,f}(T_e,\nu)}{4\pi}d\nu + \frac{W_{\nu,b}(T_e,\nu)}{4\pi}d\nu \qquad (1) \\ &= N_i\, N_e\, R\overline{v}\, \{\overline{g}(T_e,\nu) + f(T_e,\nu)\}\, \exp\left(-\frac{h\nu}{k_B T_e}\right) d\left(\frac{h\nu}{k_B T_e}\right) \\ R &= \frac{4\pi Z^2 e^6}{3^{3/2} m_e\, h\, c^3}\,,\quad \overline{v} = \sqrt{\frac{8k_B T_e}{\pi m_e}}\,. \end{aligned}$$

The quantity $\frac{W_\nu(T_e,\nu)}{4\pi}$ denotes the energy radiated per unit time, per unit volume, per steradian, per unit frequency. Similarly, $\frac{W_{\nu,f}(T_e,\nu)}{4\pi}$ and $\frac{W_{\nu,b}(T_e,\nu)}{4\pi}$ are the contributions due to free-free bremsstrahlung and radiative recombination respectively. The variables c, e, h, k_B, m_e refer to the usual physical constants.

The continuum radiation described in Eq. 1 only takes into account one species of ions. The radiation is due to two effects, both of which are quantitatively dependent on the appropriate Gaunt factors $\overline{g}(T_e,\nu)$ and $f(T_e,\nu)$. The quantity $\overline{g}(T_e,\nu)$ denotes the temperature-averaged Gaunt factor for the free-free transitions, whereas $f(T_e,\nu)$ denotes the Gaunt factor for the free-bound transitions.

The first two sections in the Appendix describe in detail how the two Gaunt factors appearing in Eq. 1 can be calculated numerically. The

core of these calculations can be found in a publication by Brussaard and van de Hulst.[21] They supply several approximations for the Gaunt factors in different regimes, as well as bibliographic references to numerical results for the regimes in which approximations are not available. Since we were interested in calculating these Gaunt factors as *continuous* functions of their parameters throughout different regimes, a combination of several approximations and numerical references were not efficient to use.

An extensive numerical calculation of Gaunt factors was also performed by Karzas and Latter.[22] Even though the theoretical background for their calculations is clearly presented, their publication does not give the details of their numerical procedures, and their final results are presented in form of graphs and are meant to be used for interpolation. Since we intend to obtain the Gaunt factors as smooth functions, we used the publication by Karzas and Latter merely as an independent cross-check for our calculations.

B. The Continuum Spectrum

For the analysis it was assumed that the deuterium ions are the only hydrogen-like ion species present in the divertor. Therefore, the two contributions to the continuum originating in the divertor are described by Eq.1. This assumption is justified since (1) we are examining the spectrum at the recombination edge of deuterium, and (2) Z_{eff} will be close to 1.0 and no other hydrogen-like species will be present for the low electron temperatures determined in the analysis. For comparison with the experimental measurements, we are interested in the continuum energy radiated per unit time, per unit volume, per steradian, per unit wavelength — a quantity which we will denote by $\frac{W_\lambda(T_e,\lambda)}{4\pi}$. It is related to Eq. 1 via

$$\frac{W_\lambda(T_e,\lambda)}{4\pi} = \frac{W_\nu(T_e,\frac{c}{\lambda})}{4\pi}\,\frac{c}{\lambda^2}\,. \tag{2}$$

We similarly denote $\frac{W_{\lambda,f}(T_e,\lambda)}{4\pi}$ and $\frac{W_{\lambda,b}(T_e,\lambda)}{4\pi}$. Having defined the emitting region in the manner described above, the spectral brightnesses B_λ observable during the actual experiment are simply related to the volume emissivities W_λ calculated from the theory via

$$B_\lambda(T_e,\lambda) = \frac{W_\lambda(T_e,\lambda)}{4\pi}\,\Delta L\,, \tag{3}$$

where ΔL is the thickness of the emitting layer. We define the quantity $\rho \equiv N_e N_i \Delta L$, such that

$$B_\lambda(T_e, \lambda) = \rho \, \frac{1}{4\pi} \frac{W_\lambda(T_e, \lambda)}{N_e N_i} \, . \tag{4}$$

In this equation ρ and T_e are the unknowns. T_e will be determined primarily from the measured change in brightness across the recombination 'edge'. This is different than what is typically done, which is to measure T_e from the slope of the continuum emission, i.e. from the $\exp(-\frac{h\nu}{k_B T_e})$ dependence of Eq. 1. The measured brightness will determine the quantity ρ. With the additional knowledge of the electron density the thickness ΔL of the 'divertor emission region' can be determined by taking N_e=N_i.

We are interested in determining the electron temperature T_e underlying the radiation due to bremsstrahlung and recombination in the 'divertor emission region'. In order to analyze our experimental data in this respect, we must first subtract the contribution of the bremsstrahlung originating in the hot core plasma. For this purpose we have used a form of Eq. 1 which includes impurities by summing over different species and the definition of Z_{eff}. We then integrate the main plasma contributions within the view by utilizing fits to the measured density and temperature profiles, $N_e^{core}(r)$ and $T_e^{core}(r)$, as well as the measured value of $Z_{eff} = 1.75$, which is constant across the main plasma. The subtraction of this brightness from the observed spectrum in Fig. 2 is done prior to all steps of the analysis described below.

Since the calculations of the continuum levels do not include the effect of the atoms' high density environment and the lowering of the energy of the 'edge', we will only use measured continuum levels for our analysis which are sufficiently separated in wavelength from the ionization limit of an isolated deuterium atom, thereby avoiding spectral regions which are most influenced by effects due to the high electron density. A tentative temperature determination can then be obtained by comparing the continuum level around $\lambda_- = 358\,\mathrm{nm}$ with the continuum level around $\lambda_+ = 452\,\mathrm{nm}$. The ratio

$$\frac{W_\lambda(T_e, \lambda_+)}{W_\lambda(T_e, \lambda_-)}$$

depends sensitively on the electron temperature T_e, as can be seen in Fig. 3.

The actual temperature determination was performed by means of a more refined procedure: six wavelengths were chosen, three on the short-wavelength side of the ionization limit for an isolated deuterium atom, and three clustered around 452 nm, a region free of contaminating lines. After subtracting the bremsstrahlung originating in the plasma core, we perform a least-squares fit of the function given on the right hand side of Eq. 4, i.e.

$$\rho R \overline{v} \frac{h c}{\lambda^2 k_B T_e} \left\{ \overline{g}\left(T_e, \frac{c}{\lambda}\right) + f\left(T_e, \frac{c}{\lambda}\right) \right\} \exp\left(-\frac{hc}{\lambda k_B T_e}\right) ,$$

to the experimental data, the $B_\lambda(T_e, \lambda)$. The constants R and $\overline{v}$ were defined in Eq. 1. The two free parameters of that fit are the divertor electron temperature T_e and the overall scale ρ defined above, which has units of $[\mathrm{m}^{-5}]$. This fit intrinsically takes into account two features of the experimental spectrum: the discontinuity of the continuum level, as well as its slope on the short-wavelength side of the spectrum. The described fit yields an electron temperature of approximately $T_e = 1.0\,\mathrm{eV}$ and an overall scale $\rho = 2.57 \cdot 10^{40}\,\mathrm{m}^{-5}$.

A comparison between the observed spectrum and the theoretically predicted continuum spectrum is shown in Fig. 4 for the electron temperatures $T_e = 0.5\,\mathrm{eV}$, $T_e = 1.0\,\mathrm{eV}$, and $T_e = 1.5\,\mathrm{eV}$. The Balmer series lines through $n \leq 11$ have been subtracted from the spectrum. For each temperature the theoretical continuum spectra were scaled to match the continuum level of the observed spectrum at wavelengths below the recombination 'edge'. Temperatures of 1.0 to 1.5 eV result in the best fit. Uncertainties in main plasma free-free bremsstrahlung contribution (the dashed-dotted line in Fig. 4) and in the relative sensitivity calibration of the spectrometer contribute to the uncertainty in the derived T_e. We estimate the maximal inaccuracy of the temperature determination to be approximately $\pm 0.5\,\mathrm{eV}$.

C. The Total Number of Radiative Recombinations

The theoretically predicted continuum spectrum due to recombination and bremsstrahlung for $Z = 1$ and $T_e = 1.0\,\mathrm{eV}$ is shown in Fig. 5. Based on the spectrum presented in Fig. 4, we intend to calculate the total rate of radiative recombination in the 'divertor emission region'. We define the symbol S_V to denote the rate of radiative recombination per unit volume.

Thus

$$S_V = \int W_{\lambda,b}(T_e, \lambda)\, \frac{\lambda}{hc}\, d\lambda, \tag{5}$$

where an integration over 4π steradians has been carried out.

Since we are interested in recombinations which lead to a deuterium atom in the ground state (see the discussion in Section V), we limit the domain of integration to $\lambda^* \leq 91.1\,\mathrm{nm}$, the wavelength corresponding to the ionization limit of the Lyman series for atomic deuterium and the recombination edge for recombination into the ground state. (This will underestimate the effective rate somewhat, because some radiative recombination into excited states will eventually decay to the ground state.) With $Z = 1$ and $T_e = 1.0\,\mathrm{eV}$, we then obtain

$$\Psi_{2bdy} = A_v\, \Delta L\, S_V \;=\; A_v\, \rho \int_0^{\lambda^*} \frac{W_{\lambda,b}(T_e, \lambda)}{N_e\, N_i}\, \frac{\lambda}{hc}\, d\lambda \;= 2.7 \cdot 10^{21} s^{-1}, \tag{6}$$

where we have used the value of ρ determined in section IV.B. If a similar computation based on $T_e = 1.5$ eV is done, a value of $\Psi_{2bdy} = 3.5 \cdot 10^{21}\,\mathrm{s}^{-1}$ results; similarly, we obtain $\Psi_{2bdy} = 1.8 \cdot 10^{21}\,\mathrm{s}^{-1}$ for $T_e = 0.5$ eV. Note that these results do not require independent knowledge of ΔL, N_e, or N_i. Only a model of the surface of the viewed 'divertor emission region' and the assumption of axisymmetry are required. However, since we have determined N_e from the Stark broadened Balmer lines, we calculate ΔL by taking $N_i = N_e$. We obtain $\Delta L = 0.033\,\mathrm{m}$, a quite reasonable value, considering the actual size of the C-Mod divertor. The thickness ΔL corresponding to modeling the emission with $T_e = 1.5$ eV and 0.5 eV are 0.05 m and 0.015 m respectively. It also does not matter that the local brightnesses may vary within the viewed area since the average brightness is measured.

V. Analysis of the Balmer Series Spectrum

In this section, the measured brightnesses of the Balmer series lines are used to show that the upper levels of the transitions are populated primarily by recombination, not by electron impact excitation from the ground state. This is demonstrated by relating the brightnesses to the emissivities and to the population densities, N_0^n, of the various excited state levels. The superscript n indicates the principal quantum number of the excited level. The measured population densities are then compared with those predicted by the collisional-radiative model of Johnson and Hinnov.[13] The confirmation that the excited levels ($n \geq 3$) are populated by recombination means that each radiative decay from those levels to the ground state represents a 'complete' recombination and is a signature thereof. This implies that one can directly measure a significant fraction of the 'complete' recombinations which occur within the field of view.

A. Dominance of Recombination

As in Section IV, we model the emission as originating from an isothermal, uniform density, axisymmetric, concentric volume of average thickness ΔL and subtended area A_v. We also assume a uniform density of neutrals in the ground state, N_0, in this volume. The brightnesses of the Balmer series lines originating from n=5 through 11 are determined from the spectrum shown in Fig. 2. A Lorentzian line shape is fit to each line. The result is plotted in Fig. 6. The entire line profiles of some of the higher n lines are not resolved since the wings of neighboring lines overlap. In those cases, the 'unseen' wings of the lines are included in the line brightnesses by integrating over the full, fitted line. In order to include the D_α brightness from the diode array with the spectrometer data in this analysis we spatially-average the D_α brightness profile over the spectrometer field of view.

The level populations are proportional to the brightnesses divided by the spontaneous emission coefficients $A_{n\to 2}$[23]:

$$N_0^n = \frac{W_{n\to 2}}{h\nu_{n\to 2}\, A_{n\to 2}} = \frac{4\pi\, B_{n\to 2}}{\Delta L\, h\nu_{n\to 2}\, A_{n\to 2}}, \tag{7}$$

where $W_{n\to 2}$ is the volume emission rate of the $n \to 2$ Balmer line, and $B_{n\to 2}$ is its brightness in units of power per unit area per steradian. As

seen in Eq. 7, the measured populations are inversely proportional to the characteristic thickness of the emission volume, a quantity determined in the last section to lie in the range 0.015 - .05 m. The measured scaling of the population densities with principal quantum number n is shown in Fig. 7. Three different values of ΔL are assumed which yield the population densities shown: a) .051 m, b) .033 m and c) .005 m. Collisional-radiative models describing the population of the excited states of hydrogen/deuterium have been constructed.[13,24,25] Johnson and Hinnov[13] show that the population density of any excited level n is given by:

$$N_0^n = N_e \left[R_n(T_e, N_e)\, N_i + E_n(T_e, N_e)\, N_0 \right], \tag{8}$$

where the first term describes population resulting from recombination. The second term describes population resulting from excitation of electrons from the atomic ground state. The coefficients[26] $R_n(T_e, N_e)$ and $E_n(T_e, N_e)$ are tabulated by Johnson and Hinnov.[13] We have used the values corresponding to the case where all of the emission lines are taken to be optically thin.

The scaling of the predicted population densities with n, based solely on the recombination term, has been calculated for N_e=8.8$\times 10^{20}$. Three different values for T_e are modeled and shown in Fig. 7a-c. At these densities and temperatures, and for n >3, the recombination term predicts population densities which are all within within 10% of the Saha-Boltzmann population densities. Also shown in each case are the population densities predicted from the excitation term only. At no T_e is the 'ground state excitation' scaling with n even close to that observed. The observed brightnesses are much better fit by the recombination scaling. *The measured population densities are clearly dominated by recombination:*

$$N_0^n \approx N_e\, N_i\, R_n(T_e, N_e), \tag{9}$$

The scaling of population densities versus n is weakly dependent upon temperature in this temperature range. The measurements are almost equally well fit by modeling T_e as 1.2 or 1.5 eV. If we demand that ΔL = 0.033 m, the value obtained from the continuum emission analysis, the fit is better for T_e=1.2 eV, at least for the principal quantum numbers $n < 7$. In both cases the theoretical prediction is lower than the measurement for n=3 (D_α), by 25% for the 1.2 eV model and by 33% for the 1.5 eV model. More will be said about D_α later.

If larger temperatures are modeled, then larger thicknesses are required to match the measured brightnesses. For example, $T_e = 2$ eV results in a scaling of the population densities, or brightnesses, with n that is as good as that for T_e=1.2 eV or T_e=1.5 eV, but a ΔL=0.08 m is required. However, this temperature is not allowed by the continuum analysis, and ΔL=0.08 m approaches the maximum, physically plausible value. For temperatures as low as 0.5 eV the fit is somewhat poorer, as seen in Fig. 7c. Note that modeling with this temperature also led to a poorer fit to the radiative recombination continuum, and the ΔL required by each analysis is different. This leads us to conclude that temperatures lower than about 0.8 eV are not allowed by the combination of both analyses. In summary, we find that, experimentally, the upper levels of the Balmer series lines are populated almost exclusively by recombination. Additionally, the temperature characteristic of the region of the Balmer line emission is in the range of from 0.8 eV to 1.5 eV.

B. Calculation of $\Psi_{n>0}$

We have previously defined $\Psi_{n>0}$ to be the rate of those 'complete' recombinations which are preceded by recombination (2- or 3-body) into excited states and which decay radiatively to the ground state. This is the recombination rate for which there is a 'signature', non-continuum photon, e.g. a Lyman series photon. Quantitatively,

$$\Psi_{n>0} = V \sum_{n>1} N_e N_i R_n(T_e, N_e) A_{n\to 1} = \rho A_v \sum_{n>1} R_n(T_e, N_e) A_{n\to 1}, \quad (10)$$

where A_v=0.72 m^2 is the area of 'divertor emission region' subtended by the view.

As long as the populations of the upper levels are dominated by recombination, $\Psi_{n>0}$ is a function of the brightnesses of the Lyman or Balmer series lines. Using equations 7 and 10,

$$\begin{aligned} \Psi_{n>0} &= 4\pi A_v \sum_{n>1} \frac{B_{n\to 1}}{h\nu_{n\to 1}} \quad (11) \\ &= A_v \left[\rho R_2(T_e, N_e) A_{2\to 1} + 4\pi \sum_{n>2} \frac{B_{n\to 2}}{h\nu_{n\to 2}} \frac{A_{n\to 1}}{A_{n\to 2}} \right]. \end{aligned}$$

The latter equality is used if the Balmer series brightnesses are measured, as in our case. Note that this latter expression does not require that the

density of the $n = 2$ level be populated primarily by recombination, since its contribution is being calculated from knowledge of N_e and T_e. This treatment can be generalized to cases where the sum over brightnesses begins at the lowest n level whose population is dominated by recombination and where the sum over $R_n A_{n\to 1}$ extends up to the n level below that. Evaluating $\Psi_{n>0}$ for T_e=1.2 eV, $N_e = N_i = 8.8 \cdot 10^{20}$ m^{-3} and $\Delta L = 0.033$ m, we obtain

$$\Psi_{n>0} = 4.4 \cdot 10^{22}\,\mathrm{s}^{-1}(\text{Eq. 10}) \text{ and } \Psi_{n>0} = 4.6 \cdot 10^{22}\,\mathrm{s}^{-1}(\text{Eq. 11}). \qquad (12)$$

Ly_α accounts for about $\approx$65% of this rate. This contribution was not measured in our case, but is, in principle, measurable. For 0.8 eV$< T_e <$ 1.5 eV we obtain $4.3 \cdot 10^{22}\,\mathrm{s}^{-1} < \Psi_{n>0} < 5.7 \cdot 10^{22}\,\mathrm{s}^{-1}$. Note that the recombination rates $\Psi_{photonless}$ and Ψ_{2bdy}, as defined, are not included in this total.

Before leaving the details of the Balmer series spectrum, we speculate about the difference between the measured and predicted population density for the n=3 level. The 30% discrepancy (more population observed than predicted by recombination alone) is not within the estimated error of the relative intensity calibration between the D_α array and the spectrograph. A plausible explanation is that the higher measured population density is a result of a contribution by excitation from ground state atoms. At a 1.2 eV temperature, a ground state neutral density in the 'divertor emission region' of $N_0 = 4 \cdot 10^{21}$ m^3 is required to raise the predicted N_0^3 density to the measured value. This neutral density is much higher (10^2) than that inferred from pressure measurement of D_2 in the divertor. This high neutral density may be possible, but we have no measurement to support it. We therefore consider several other possibilities.

It is reasonable to expect that there is a region of higher temperature in the view where ground state neutrals still exist. If, for example, there is a 5eV, $N_e = 2 \cdot 10^{20}$ m^3 region of thickness 0.005 m between the divertor and the main plasma, a more plausible neutral density of $7.4 \cdot 10^{19}$ m^3 is required to raise the n=3 population density to that measured. These arguments can be understood with reference to the excitation-only curves in Fig. 7, which show that excitation can affect the n=3 population density without affecting the higher-n states. A second possible explanation of the enhanced n=3 density is that it is a result of recombination through vibrationally excited deuterium molecules.[10,11,9] This process preferentially populates the n=3,4 levels. We cannot choose between these possibilities based upon the present experimental observations. However, we note that no moleculular

lines have been observed, either in the visible or the VUV. In addition, for reasons discussed in Section VI.B, contributions from the excitation process are probably not negligible. A fourth possible scenario is that, of the Lyman series, Ly_α is optically thick, leading to an enhanced population density for n=2 which would preferentially increase the population density for n=3, and thereby increasing D_α and Ly_β. We have no capability, at this time, of quantitatively evaluating this effect.

VI. Discussion

In the preceding sections, we have analysed two aspects of the measured visible spectrum, the radiative recombination/bremsstrahlung continuum and the Balmer series lines, with the goal of diagnosing the types and amount of recombination in the C-Mod divertor plasma. Although the spectroscopic signatures (continuum and line emission) are different, the physics giving rise to the photons measured is intimately related and must therefore give consistent results. The analyses determined an electron temperature T_e and density N_e characteristic of a 'divertor emission region', assumed to be isothermal and of uniform density, with average thickness ΔL. In the following we will discuss the overall consistency of these results and calculate the *total* rate of 'complete' recombination. That rate is then compared to the other sink for plasma ions, ion flow to the divertor plates. We do this in order to quantify the importance of recombination to divertor physics. In addition, we will discuss the uncertainties of the analysis.

A. The Total Recombination Rate and the Consistency of the Data

Each of the analyses detailed in sections IV and V results in sets of matched pairs of T_e and ΔL which bracket the experimental measurements. In section V we point out that these sets are consistent only over a fairly narrow range 0.8 eV$\leq T_e \leq$1.5 eV. We have thus used this consistency between the 2 different methods to arrive at our best determination of T_e.

In Sections IV.C and V.B, the total rate of radiative recombinations to the ground state, Ψ_{2bdy}, as well as the total rate of 'complete' recombinations for which there are 'signature' photons, $\Psi_{n>0}$, were determined. The only recombination process for which we have not accounted is three-body recombination which results in a ground state atom but which has decayed to the ground state from an excited state by collisional de-excitation. We associate this process with the rate $\Psi_{photonless}$. $\Psi_{photonless}$ cannot be measured spectroscopically, but can be calculated based on the knowledge of temperature and density. The overall rate coefficient for 'complete' recombinations, $\langle\sigma v\rangle_{rec}$, has been calculated, for example, by various authors.[13,10] Using either of the rates from these references and taking $T_e = 1.2\,\mathrm{eV}$ and $N_e = 8.8 \cdot 10^{20}\,\mathrm{m}^{-3}$, we obtain

$$\langle \sigma v \rangle_{rec} \approx 2.9 \cdot 10^{-18}\,\mathrm{m^3\,s^{-1}}, \tag{13}$$

leading to a total rate of 'complete' recombinations given by

$$\Psi_{rec} = 5.3 \cdot 10^{22}\,\mathrm{s^{-1}} = \Psi_{photonless} + \Psi_{n>0} + \Psi_{2bdy}. \tag{14}$$

This result implies that $\Psi_{photonless}$ constitutes $\leq$10% of the total since the sum of the last two terms have been determined to be $\approx 5 \cdot 10^{22}\,\mathrm{s^{-1}}$. This calculation of the total recombination rate could have been made as soon as the temperature, density, and viewing geometry are known. However, the characteristic time for a 'complete' recombination to occur can be of the same order as the transit time of ions through the divertor region. Thus the underlying transport must be considered when relying merely on the determination of N_e and T_e. Measurement of 'signature' recombination photons is a measurement of recombinations that actually occur, and therefore a more direct measurement of the 'complete' recombination rate.

B. Relevance of Recombination

To gauge the relative importance of recombination among the processes occurring in the divertor region, we compare its magnitude with the other sink for ions, the ion current to the divertor plates. In addition, the ion sources (ionization) must balance the ion sinks. Typically the ionization rate is inferred from the D_α emission,[13,24] assuming an *ionizing* plasma. This condition does not apply in the present case, since we have already determined that the D_α emission is primarily a result of recombination. Thus the ionization sources are not measured directly, and we are left to show that the required ion source rate is consistent with the spectral measurements of the Balmer series.

The rate of ions striking the plates has been inferred from measurements made with arrays of Langmuir probes mounted in the inner and outer divertor plates.[4] The total ion current to the plates, which is the sum of the currents striking inner and outer divertor plates, is

$$I_{tot} \;=\; I_{inner} + I_{outer} \approx 1 \cdot 10^{22}\,\mathrm{s^{-1}} + 6 \cdot 10^{22}\,\mathrm{s^{-1}}. \tag{15}$$

Thus,

$$\frac{\Psi_{rec}}{I_{tot}} \sim 0.8, \tag{16}$$

meaning that *roughly 1/2 to 1/3 of all ions recombine before they reach the divertor plates.* Under conditions achieved in the detached Alcator C-Mod divertor, recombination plays a major role in the particle balance. Recent modeling of the Alcator C-Mod divertor plasma agrees with this observation.[27]

In order to maintain the particle balance, we require that the total number of ionizations, Ψ_{ion}, balance the total sink, i.e.

$$\Psi_{ion} = I_{tot} + \Psi_{rec} \approx 7 \cdot 10^{22}\,\mathrm{s}^{-1} + 5 \cdot 10^{22}\,\mathrm{s}^{-1}. \tag{17}$$

Thus the divertor region must be supplied with ions at rate of $\sim 1 \cdot 10^{23}\,\mathrm{s}^{-1}$. If we assume that this source is in the field of view and is not transported to the divertor plates from regions outside the field of view, then we find that the measured temperature and density in the 'divertor emission region' do not engender the required ionization source without a very large neutral density. N_0 of $\sim 6 \cdot 10^{21}\,\mathrm{m}^{-3}$ would be required, since

$$\Psi_{ion} = N_0\, N_e\, \langle \sigma v \rangle_{ioniz}\, A_v \Delta L, \tag{18}$$

and $\langle \sigma v \rangle_{ioniz}$ is so small[13] ($\sim 8 \cdot 10^{-19}\,\mathrm{m}^3\,\mathrm{s}^{-1}$) for $T_e = 1.2$ eV. However, as argued in Section V, there is an alternative explanation - an ionizing region of higher T_e in the field of view can supply the required source without significantly influencing the measured Balmer spectrum. Finally, we note that the ionization rate is not easily measured in these conditions.

C. The Assumptions of Uniform T_e and N_e in the Emission Region

Because temperature and density are derived from the analyses of the same lines which are used to determine the recombination rate, there is not the uncertainty of associating the emission with an independently measured temperature or density profile. In other words, this result is not derived from a combination of measurements from different diagnostics. The Balmer lines, which yield a determination of the recombination rate, also yield the *most appropriate* density in the environment from which they arise (through

the Stark broadening analysis). In addition, we note that any uncertainties resulting from the Stark broadening analysis or arising from a distribution of densities which give rise to the measured line shape do not significantly influence the recombination determination. In the same way, the continuum spectrum yields the *most appropriate* temperature in the environment from which the radiative recombination arises.

The effects of uncertainties in density and temperature on the total 'complete' recombination rate are minimized if one directly measures the available 'signature' photons. See Eq. 11, for example, which indicates that, if the levels are populated primarily by recombination and if the Lyman series brightnesses are measured, then the evaluation of $\Psi_{n>0}$ does not depend on the spatial distribution of density and temperature within the field-of-view. The major fraction of the 'complete' recombination rate is strictly dependent on the line brightnesses and on the area subtended by the emitting region. However, since not all 'complete' recombinations are observed, even indirectly through line emission, the effects on the total recombination rate of different temperatures within the view must be addressed. A concise way of quantifying this is to relate the total recombination rate to local brightnesses, B_{n^*} of the Lyman or Balmer series lines whose upper levels, n^*, are populated by recombination. This can be expressed as

$$\Psi_{rec} = 4\ \pi\ C_{n^*} \cdot \sum_{n^*} \int_{field-of-view} \frac{B_{n^*}}{h\nu}\ dA. \tag{19}$$

C_{n^*} is a coefficient which includes the contributions to the recombination rate which are not measured directly, e.g. $\Psi_{photonless}$, Ψ_{2bdy}, or recombination-populated density of n=2 when the Ly_α brightness is not measured. We have evaluated C_{n^*} as a function of different, but uniform, temperatures and for fixed density in the recombination region. Two scenarios were investigated: assuming the Lyman series ($n^* \geq 2$) brightnesses have been measured, and assuming, as in our case, that only the Balmer series ($n^* \geq 3$) brightnesses have been measured. In both cases the emission is taken to be due to recombination only. We find that C_{n^*} varies little over a range in temperature from 0.5 - 3.0 eV. From this we conclude that, even if the emitting region is inhomogeneous, there is little error brought about by assuming a single T_e (10-25% uncertainty).

D. Relative Importance of Different Recombination Pathways

The rates for the different recombination processes have already been presented, and we summarize them here to show their relative importance: At the temperature and density characterizing the divertor emission region, $\sim$ 90% of the total number of 'complete' recombinations results in the emission of Lyman series photons, which are in principle measurable. These photons are the result of decays from excited states which are populated primarily by 3-body recombination. Another $\sim$5% occurs as radiative recombination to the ground state and is accompanied by the emission of a continuum photon of energy >13.6 eV. These also are measureable. The final $\sim$5% starts as 3-body recombination into excited states and ends in the ground state after collisional de-excitation. There is no 'signature' photon. As discussed in Section V, some relatively small fraction of recombination occurring via excited molecules is allowed by the measurements, but there is no definitive signature in these observations.

VII. Summary

The visible spectrum from a detached divertor plasma in Alcator C-Mod has been analyzed. Densities and temperatures in the emitting region were determined. The Balmer series spectrum was seen to be a result of upper level population densities which are close to those predicted by a Saha-Boltzmann distribution, meaning that recombination is the dominant population mechanism of these excited states. As a result, a large fraction of the total recombination rate was determined spectroscopically. Recombination, occurring in the divertor region, was shown to play a significant role in the removal of ions from the plasma.

Acknowledgements

The authors gratefully acknowledge the assistance of the entire Alcator C-Mod group, without which this study could not have occurred. We thank D. Pappas for his assistance with the spectrometer. We also thank Professor Ian Hutchinson, Dr. S. Krasheninnikov, Professor T. Fujimoto, Professor K. Sawada, Dr. D. Post and Dr. Y. Pigarov for very helpful discussions.

Support for this work was provided from the U.S. Department of Energy under contract number DE-AC02-78ET51013.

Appendix A. Calculational Details

In this appendix, we describe a calculational approach which can be straightforwardly applied to calculate the intensity of the continuum radiation due to bremsstrahlung and recombination. Employing several techniques to render the procedure more time-efficient, this description is meant to provide the means for a direct conversion into a code operational on a computer.

We denote bound states by the quantum numbers $n, n' \in \mathbb{N}$, with $\mathbb{N}$ being the set of positive non-zero integers. These quantum numbers are related to the energy eigenvalues of these discrete states via

$$E(n) = -\frac{h\nu_0 Z^2}{n^2}\,. \tag{A1}$$

Continuum states are denoted by the parameters $\eta, \eta' \in \mathbb{R}$, with $\mathbb{R}$ denoting the set of real numbers. Analogous to n and n', the corresponding energy levels are expressed by

$$E(i\eta) = +\frac{h\nu_0 Z^2}{\eta^2}\,. \tag{A2}$$

Here, ν_0 denotes the ionization frequency from the ground state of atomic hydrogen with $Z = 1$. The parameters E', n', and η' will exclusively be used to refer to the final state of a transition. In general, the relation

$$\begin{aligned} \nu(k,k') &= \nu_0 Z^2 \left(\frac{1}{k'^2} - \frac{1}{k^2}\right), \\ & k = n \text{ or } k = i\eta\,,\ \ k' = n' \text{ or } k = i\eta'\,, \end{aligned} \tag{A3}$$

is used for relating the photon frequency ν to the parameters describing the transition.

Evaluating the Gaunt Factor for the Free-Free Transitions

The Gaunt factor g for a transition between the initial continuum energy level with $E = h\nu_0 Z^2/\eta^2$ and the final continuum state with $E' = h\nu_0 Z^2/\eta'^2$ is expressed as

$$g(\eta,\eta') = \frac{\sqrt{3}\,L(\eta,\eta')}{\pi}\,. \tag{A4}$$

$L(\eta,\eta')$ can be written[21]:

$$L(\eta,\eta') = \frac{\pi^2\,\eta\,\eta'}{(e^{2\pi\eta}-1)(1-e^{-2\pi\eta'})}\,\frac{|\Delta(i\eta,i\eta')|}{\eta'-\eta}\,. \tag{A5}$$

It is stated there that this result is quantum mechanically rigorous in the non-relativistic case and equivalent to another expression for $L(\eta,\eta')$ which was derived by Sommerfeld and Maue. The function $\Delta(k,k')$ can be calculated[28]:

$$\begin{aligned}\Delta(k,k') &= \{F(-k+1,-k',1;x)\}^2 - \{F(-k'+1,-k,1;x)\}^2\,, \\ x &= -\frac{4\,k\,k'}{(k-k')^2}\,,\end{aligned} \tag{A6}$$

where $F(a,b,c;x)$ denotes the hypergeometric function.

Within the unit circle of the complex plane $|x|<1$, the function $F(a,b,c;x)$ can be expressed (see Erdelyi[29]) by the series

$$F(a,b,c;x) = 1 + \frac{a\,b}{c}\,\frac{x}{1!} + \frac{a(a+1)\,b(b+1)}{c(c+1)}\,\frac{x^2}{2!} + \cdots\,. \tag{A7}$$

For $|x|<0.95$, this function was evaluated directly. The series was taken to have converged when the absolute value of the last term was smaller than 10^{-6}. When this criterion was not fulfilled after summing 150 partial terms, the function was not evaluated for the given parameters.

For $|x|>1.05$, the analytic continuation of the hypergeometric function was used, which is given as[30]:

$$\begin{aligned}F(a,b,c;x) &= \frac{\Gamma(c)\Gamma(b-a)}{\Gamma(b)\Gamma(c-a)}(-x)^{-a}F(a,1-c+a,1-b+a;x^{-1}) \\ &\quad + \frac{\Gamma(c)\Gamma(a-b)}{\Gamma(a)\Gamma(c-b)}(-x)^{-b}F(b,1-c+b,1-a+b;x^{-1})\,, \\ &\quad \text{with } a,b,c,x \in \mathbb{C}\,.\end{aligned} \tag{A8}$$

This analytic continuation involves the evaluation of the Gamma function for values from the entire complex plane. For the domain

$$\{x | x \in \mathbb{C},\ 0.95 < |x| < 1.05\}\,,$$

the hypergeometric function was not evaluated. In this case the Gaunt factor was not calculated.

The approach by Lanczos was employed for evaluating the complex Gamma function:

$$\Gamma(z+1) = \left(z+\gamma+\frac{1}{2}\right)^{z+\frac{1}{2}} e^{-(z+\gamma+\frac{1}{2})} \cdot\sqrt{2\pi}\left[c_0+\frac{c_1}{z+1}+\frac{c_2}{z+2}+\ldots+\frac{c_N}{z+N}+\epsilon\right]\,;\,\mathrm{Re}\,z>0\,. \tag{A9}$$

For $\gamma = 5$ and $N = 6$, this method is described elsewhere,[31] where the necessary coefficients c_i; $i \in \{0,\ldots,6\}$ are supplied as well. This procedure allows calculation of the values of the complex Gamma function with an error smaller than $|\epsilon| < 10^{-10}$ in the entire half complex plane $\mathrm{Re}\,z > 0$. The same reference also provides a reflection formula which allows one to calculate $\{\Gamma(z)|z \in \mathbb{C},\ \mathrm{Re}\,z < 1\}$ from $\{\Gamma(z)|z \in \mathbb{C},\ \mathrm{Re}\,z > 1\}$.

With the information provided so far, it is possible to calculate the Gaunt factor $g(E,\nu)$ for a free-free transition. Equ. 1 requires the knowledge of the temperature averaged Gaunt factor $\overline{g}(T,\nu)$, which can be calculated[21]:

$$\overline{g}(T,\nu) = \int_{E'=0}^{\infty} g(E'+h\nu,\nu)\, e^{-\frac{E'}{k_B T}}\, d\left(\frac{E'}{k_B T}\right)\,. \tag{A10}$$

For the evaluation of this integral, a quadrature formula was used:

$$\int_0^{\infty} e^{-x} f(x)\, dx = \sum_{j=1}^{q} a_j\, f(x_j)\,. \tag{A11}$$

Such a method is described by Chandrasekhar.[32] We employed this calculational approach with $q = 5$, for which the corresponding $\{a_j, x_j | j \in \{1,\ldots,5\}\}$ are presented in the same reference.

Evaluating the Gaunt Factor for the Free-Bound Transitions

The quantity $f(T,\nu)$ refers to the Gaunt factor for the transitions from the free continuum level with the energy $E = h\nu_0 Z^2/\eta^2$ to the bound level with the energy $E' = -h\nu_0 Z^2/n'^2$. We can express $f(T,\nu)$ as[21]:

$$f(T,\nu) = 2\theta \sum_{n=m}^{5} g_n \frac{e^{\theta/n^2}}{n^3} \tag{A12}$$

$$+2\,\theta g_\infty \sum_{n=6}^{\infty} \frac{e^{\theta/n^2}}{n^3} + 50\,\theta\,(g_5 - g_\infty) \sum_{n=6}^{\infty} \frac{e^{\theta/n^2}}{n^5}\,,$$

$$\theta \;=\; \frac{h\nu_0 Z^2}{k_B T}\,,$$

The first term within this sum is dependent on $m = m(\nu)$, the lowest principal quantum number among the energy levels accessible with a given frequency ν. The functions $g_{n'}(\nu)$ occurring in Eq. A12 denote the Gaunt factor for the transition from the continuum state with the energy $E = -h\nu_0 Z^2/n'^2 + h\nu$ to the bound state with the energy $E' = -h\nu_0 Z^2/n'^2$. They are defined[28]:

$$g_{n'}(\nu) = \frac{\pi\sqrt{3}\,\eta\,n'}{\sqrt{\eta^2 + n'^2}\,(1 - e^{-2\pi\eta})}\, e^{-4\eta \arctan(\frac{n'}{\eta})}\, |\Delta(i\eta, n')|\,, \qquad \text{(A13)}$$

where $\Delta(i\eta, n')$ can be calculated from Eq. A6 and where Eq. A3 is used for relating ν to η and n'. For the calculation of g_∞ appearing in Eq. A12 , we take advantage of the approximation

$$g_n = g_\infty + \frac{64}{n^2}(g_8 - g_\infty) \;\text{ with}\, n = 12\,, \qquad \text{(A14)}$$

which represents a slight modification of what is found in Brussard and Hulst.[21]

Independent Verification of Numerical Results

The entire calculation was performed by a code written in IDL employing double precision variables. The results obtained for the temperature averaged free-free Gaunt factor $\overline{g}$ are consistent with Karzas and Latter.[22] The results for the functions $g_{n'}(\nu)$ resemble those determined by Brussaard and Hulst.[21] The overall continuum spectrum due to both recombination and bremsstrahlung also agrees with previous calculations.[21]

References

[1]P.C. Stangeby, *Nuclear Fusion*, **33**, 1695 (1993).

[2]K. Borrass and G. Janeschitz, *Nuclear Fusion*, **34**, 1203 (1994).

[3]J.A. Goetz, C. Kurz, B. LaBombard, B. Lipschultz, A. Niemczewski, G.M. McCracken, J.L. Terry, R. Boivin, F. Bombarda, P. Bonoli, C. Fiore, S. Golovato, R. Granetz, M. Greenwald, S. Horne, A. Hubbard, I.H. Hutchinson, J. Irby, E. Marmar, M. Porkolab, J. Rice, J. Snipes, Y. Takase, R. Watterson, B. Welch, S. Wolfe, C. Christenson, D. Garnier, D. Jablonski, D. Lo, D. Lumma, M. May, A. Mazurenko, R. Nachtrieb, P. O'Shea, J. Reardon, J. Rost, J. Schachter, J. Sorci, P. Stek, M. Umansky, and Y. Wang, *Phys. of Plasmas*, **3**, 1908 (1996).

[4]B. LaBombard, J.A. Goetz, C. Kurz, D. Jablonski, B. Lipschultz, G.M. McCracken, A. Niemczewski, R. Boivin, F. Bombarda, P. Bonoli, C. Christenson, S. Fairfax, C. Fiore, D. Garnier, M. Graf, S. Golovato, R. Granetz, M. Greenwald, S. Horne, A. Hubbard, I.H. Hutchinson, J. Irby, J. Kesner, T. Luke, E. Marmar, M. May, P. O'Shea, M. Porkolab, J. Reardon, J. Rice, J. Schacter, J. Snipes, P. Stek, Y. Takase, J.L. Terry, G. Tinios, R. Watterson, B. Welch, and S. Wolfe, *Physics of Plasmas*, **2**, 2242 (1995).

[5]S. L. Allen, D. N. Hill, T. N. Carlstrom, D.G. Nilson, T.W. Petrie, A.W. Leonard, D. Ryutov, G.D. Porter, R. Maingi, M.R. Wade, R.H. Cohen, W.M. Nevins, M.E. Fenstermacher, R.D. Wood, C.J. Lasnier, W.P. West, and M.D. Brown, *Measurements of Electron Temperature and Density With DTS in Radiative Divertor Discharges in DIII-D*, Proceedings of the 12th Plasma Surface Interactions Conference, St. Raphael, France, May 1996, to be published in the J. Nucl. Mater., Paper B37.

[6]A. Loarte, *Understanding the Edge Physics of Divertor Experiments by Comparison of 2-D Edge Code Calculations and Experimental Measurements*, Proceedings of the 12th Plasma Surface Interactions Conference, St. Raphael, France, May 1996, To be published in the J. Nucl. Mater., Paper I-09.

[7]K. Borrass, D. Coster, D. Reiter, and R. Schneider, *Study of Recombining Gas Targets*, Proceedings of the 12th Plasma Surface Interactions Con-

ference, St. Raphael, France, May 1996, To be published in the J. Nucl. Mater., Paper A41.

[8]G.F. Matthews, *J. Nucl. Materials*, **220-222**, 104 (1995).

[9]S. I. Krasheninnikov, A. Yu. Pigarov, T. K. Soboleva, and D. J. Sigmar, *Plasma-Neutral Gas Interaction in a Tokomak Divertor: Effects of Hydrogen Molecules and Plasma Recombination*, Proceedings of the 12th Plasma Surface Interactions Conference, St. Raphael, France, May, 1996. to be published in J. of Nucl. Materials, Paper A-47.

[10]R. K. Janev, D.E. Post, W.D. Langer, K. Evans, D.B. Heifetz, and J.C. Weisheit, *J. Nucl. Mater.*, **121**, 10 (1984).

[11]D.E. Post, *J. Nucl. Materials*, **220-222**, 143 (1995).

[12]R. W. McWhirter, *Plasma Physics and Nuclear Fusion Research, edited by R.D. Gill*, chapter 10, Academic Press, 1981.

[13]L. C. Johnson and E. Hinnov, *J. Quant. Spectrosc. Radiat. Transfer*, **13**, 333 (1973).

[14]ITER-JCT and Home Teams, *Plasma Phys. and Control. Fusion*, **37**, A19 (1995).

[15]I. H. Hutchinson, R. Boivin, F. Bombarda, P. Bonoli, S. Fairfax, C. Fiore, J. Goetz, S. Golovato, R. Granetz, M. Greenwald, S. Horne, A. Hubbard, J. Irby, B. LaBombard, B. Lipschultz, E. Marmar, G. McCracken, M. Porkolab, J. Rice, J. Snipes, Y. Takase, J. Terry, S. Wolfe, C. Christenson, D. Garnier, M. Graf, T. Hsu, T. Luke, M. May, A. Niemczewski, G. Tinios, J. Schachter, and J. Urbahn, *Physics of Plasmas*, **1**, 1511 (1994).

[16]J. L. Terry, J. A. Snipes, and C. Kurz, *Rev. Sci. Instrum.*, **66**, 555 (1995).

[17]C. Kurz, J. A. Snipes, J. L. Terry, B. LaBombard, B. Lipschultz, and G.M. McCracken, *Rev. Sci. Instrum.*, **66**, 619 (1995).

[18]B. L. Welch, H.R. Griem, J.L. Terry, C. Kurz, B. LaBombard, B. Lipschultz, E. Marmar, and G. McCracken, *Physics of Plasmas*, **2**, 4246 (1995).

[19]D. Lumma, *Investigation of a Diagnostic Technique for Measuring Electron Densities via Stark Broadening on the Alcator C-Mod Tokamak*, Thesis for the MSc degree in Physics, Massachusetts Institute of Technology, 1996.

[20]D. R. Inglis and E. Teller, *The Astrophysical Journal*, **90**, 439 (1939).

[21]P. J. Brussaard and H. C. van de Hulst, *Reviews of Modern Physics*, (1962).

[22]W. J. Karzas and R. Latter, Electron Radiative Transitions in a Coulomb Field, The Rand-Corporation Research Memorandum RM-2010-AEC, ASTIA Document Number AD1560461 (unpublished), 1957/1958.

[23]W. L. Wiese, M. W. Smith, and B. M. Glennon, *Atomic Transition Probablilities*, National Standard Reference Data Series - NBS-4, U.S. Gov. Printing Office, Washington, D.C., 1966.

[24]T. Fujimoto, S. Miyachi, and K. Sawada, *Nucl. Fus.*, **28**, 1255 (1988).

[25]A.Yu. Pigarov and S.I. Krasheninnikov, *Application of Collisional-radiative and atomic-molecular model to the recombining divertor plasma*, To appear in Phys. Let. A, 1996.

[26]In the notation of Johnson and Hinnov,[13] where $p \equiv n$, $n(H^+) \equiv N_i$, and $n(1) \equiv N_0$:

$$N_i\ N_e\ R_p(T_e, N_e) = r_0(p)\ \ n_E(p) \quad \text{and} \quad N_e\ E_p(T_e, N_e) = r_1(p)\ \frac{n_E(p)}{n_E(1)}$$

.

[27]F. Wising, D.A. Knoll, S.I. Krasheninnikov, T.D. Rognlien, and D.J. Sigmar, *Contrib. Plasma Phys.*, **36**, 136 (1996).

[28]D. H. Menzel and C. L. Pekeris, *Monthly Notices Roy. Astron. Soc.*, **96**, 77 (1935).

[29]A. Erdélyi, *Higher Transcendental Functions*, McGraw-Hill, New York, 1953, Vol. I. Bateman Manuscript Project, California Institute of Technology.

[30]J. M. Berger, *Physical Review*, **105**, 35 (1957).

[31]W. H. Press, B. P. Flannery, S. A. Teukolsky, and W. T. Vetterling, *Numerical Recipes in C*, Cambridge University Press, Cambridge, 1988.

[32]S. Chandrasekhar, *Radiative Transfer*, Dover Publications, Inc., New York, 1960.

Appendix B. Figures

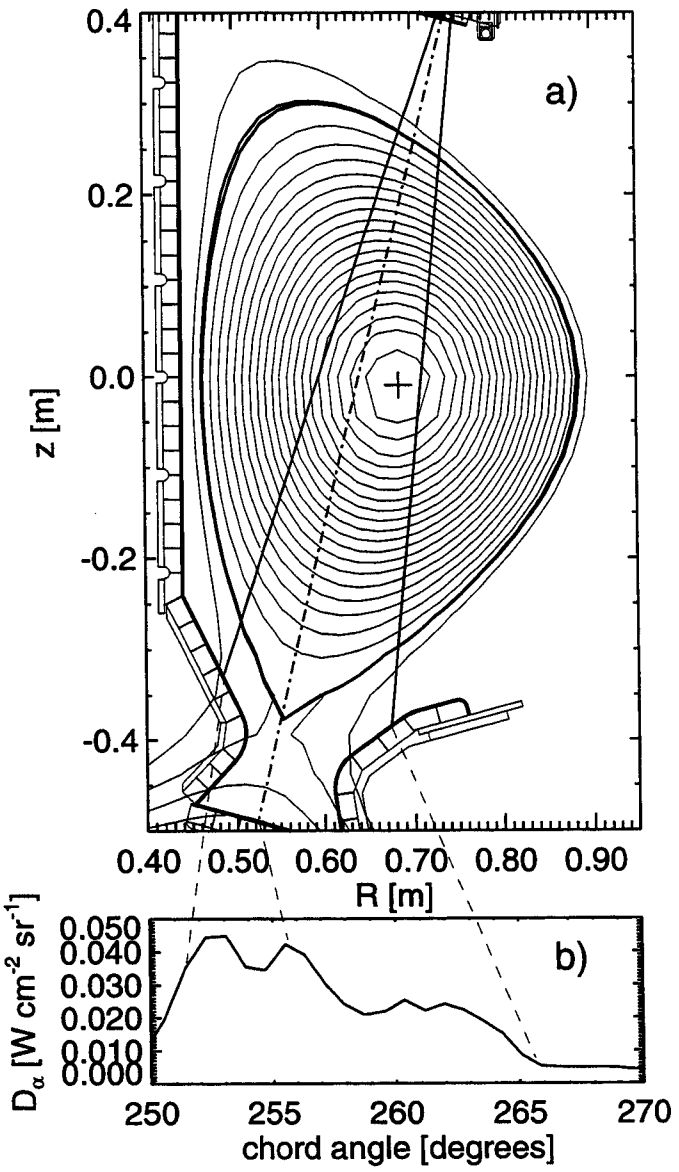

Figure 1: (a) A poloidal cross-section of the Alcator C-Mod tokamak showing the field of view of the spectrometer. (b) The D_α brightness profile observed as a function of the chord angle with the diode array.

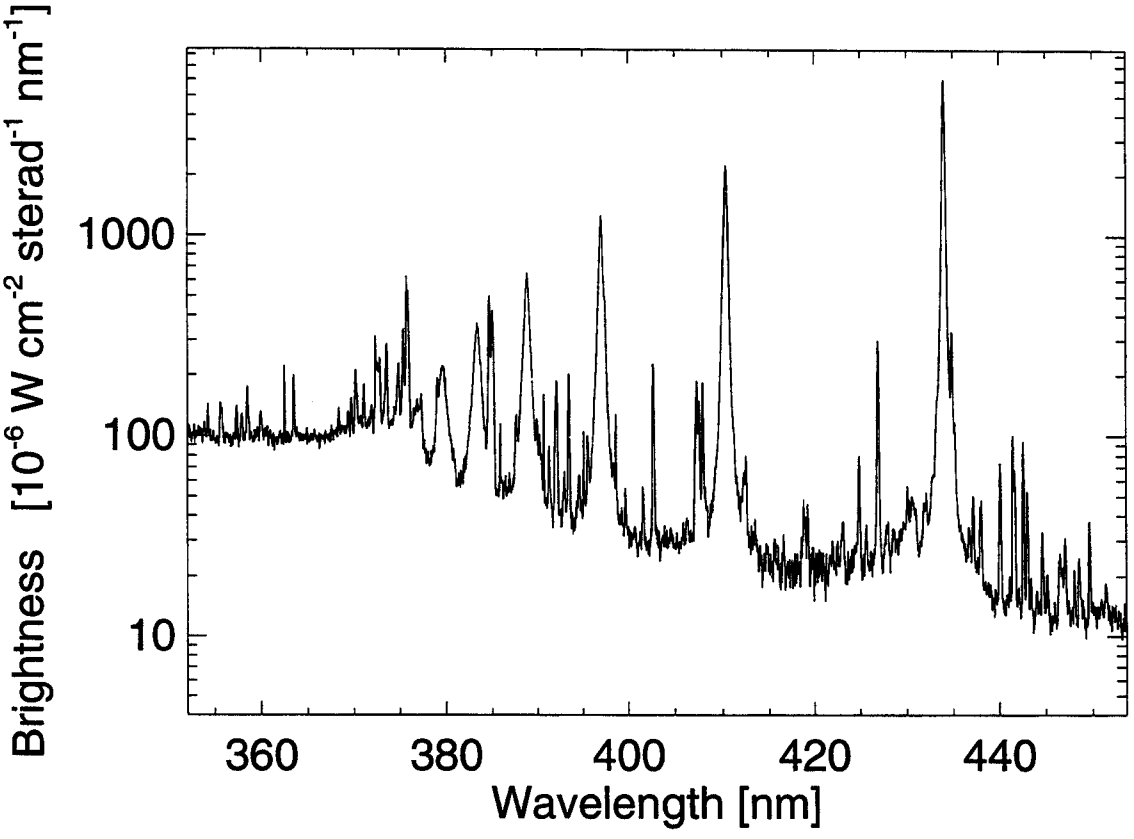

Figure 2: Spectrum from around the Balmer series limit obtained from three identical discharges. The spectrum is measured between 0.917 s and 0.979 s after the start of the discharge.

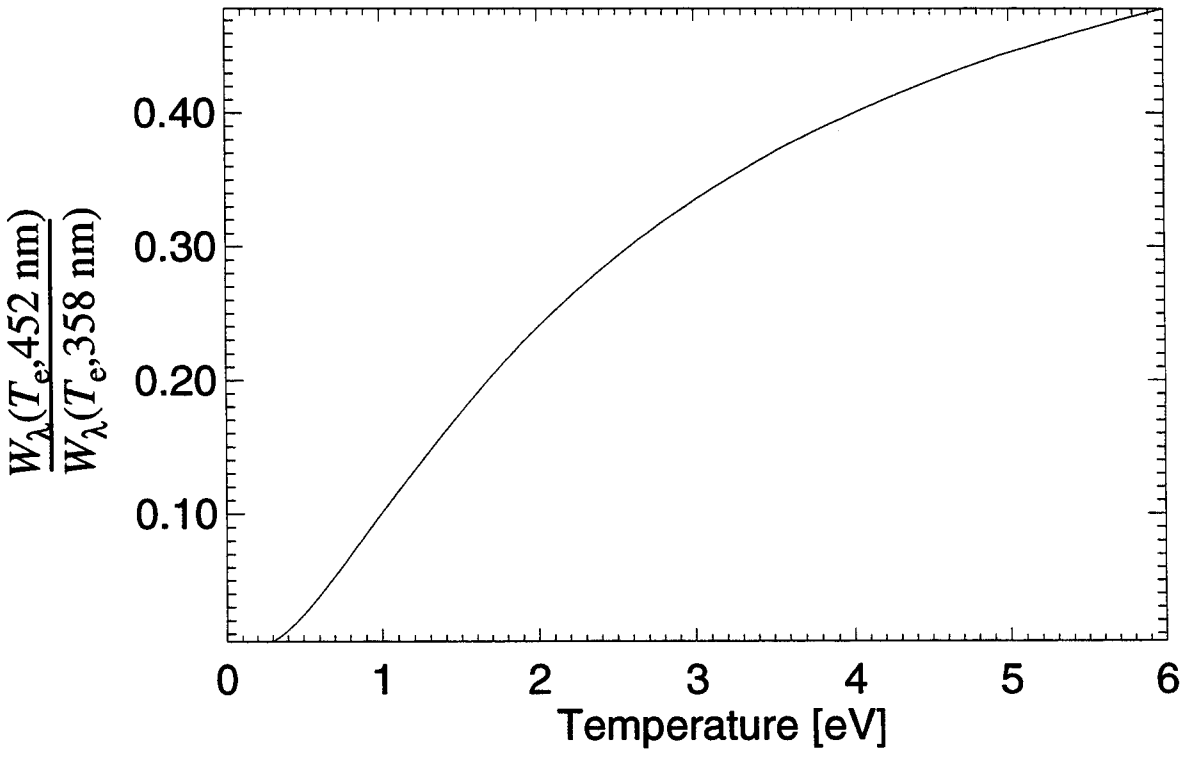

Figure 3: The predicted temperature dependence of the continuum emissivity ratio $\frac{W_\lambda(T_e,452nm)}{W_\lambda(T_e,358nm)}$ for $Z = 1$.

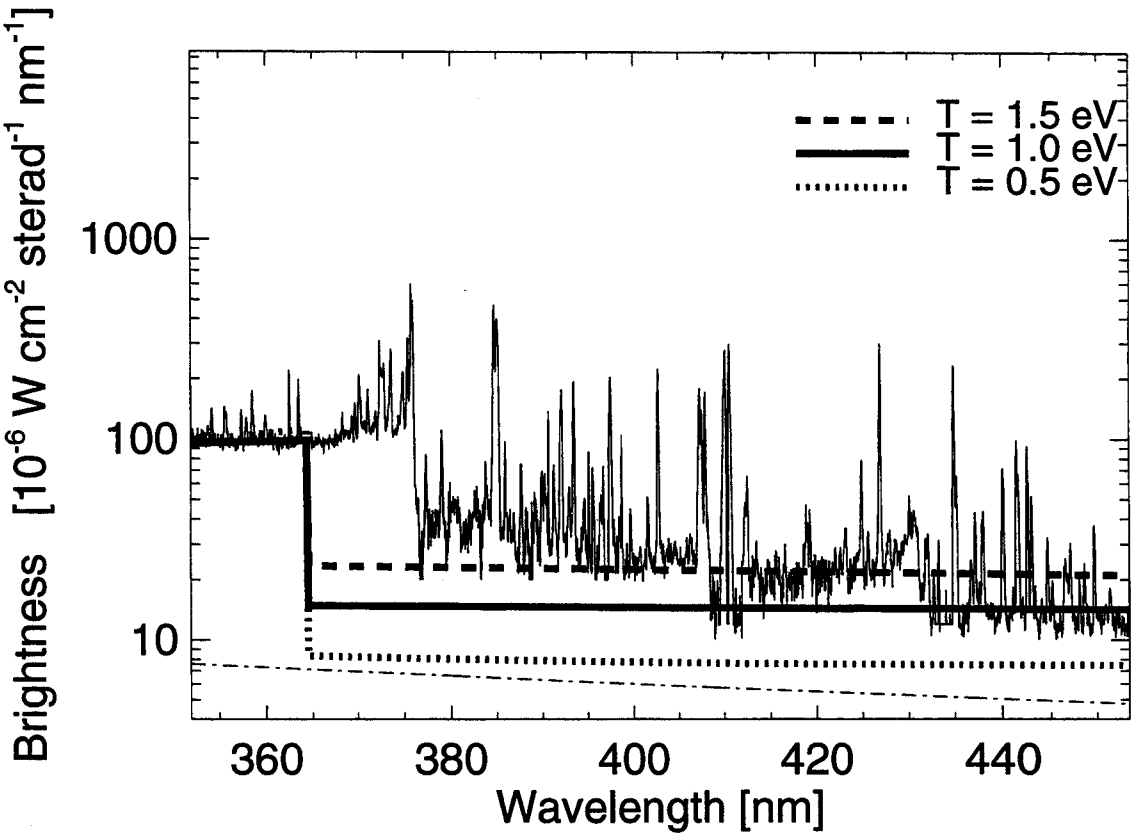

Figure 4: The recombination 'edge' and its sensitivity to the temperature: The Balmer series lines have been subtracted from the spectrum of Fig. 2. Superposed are the theoretically predicted continuum spectra due to bremsstrahlung and radiative recombination for three different electron temperatures. Note that the theoretical continuum spectra were scaled *separately* to match the low wavelength continuum. The lower dashed-dotted line indicates the calculated bremsstrahlung contribution from the core of the plasma.

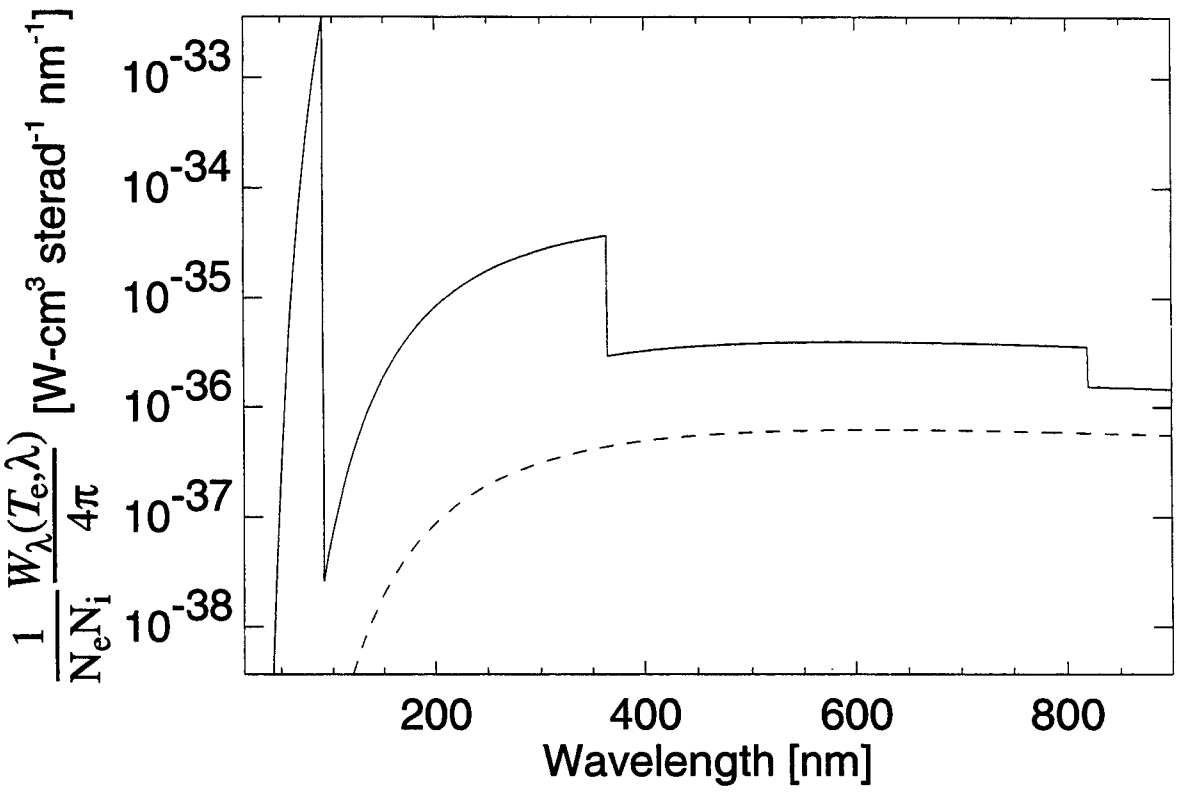

Figure 5: Theoretically predicted continuum due to radiative recombination and bremsstrahlung: The solid line denotes the continuum spectrum $\frac{1}{N_e N_i}\frac{W_\lambda(T_e,\lambda)}{4\pi}$ due to both radiative recombination and bremsstrahlung as a function of λ for $Z = 1$ and $T_e = 1.0\,\mathrm{eV}$. The dotted curve shows the contribution to this continuum which is solely due to bremsstrahlung.

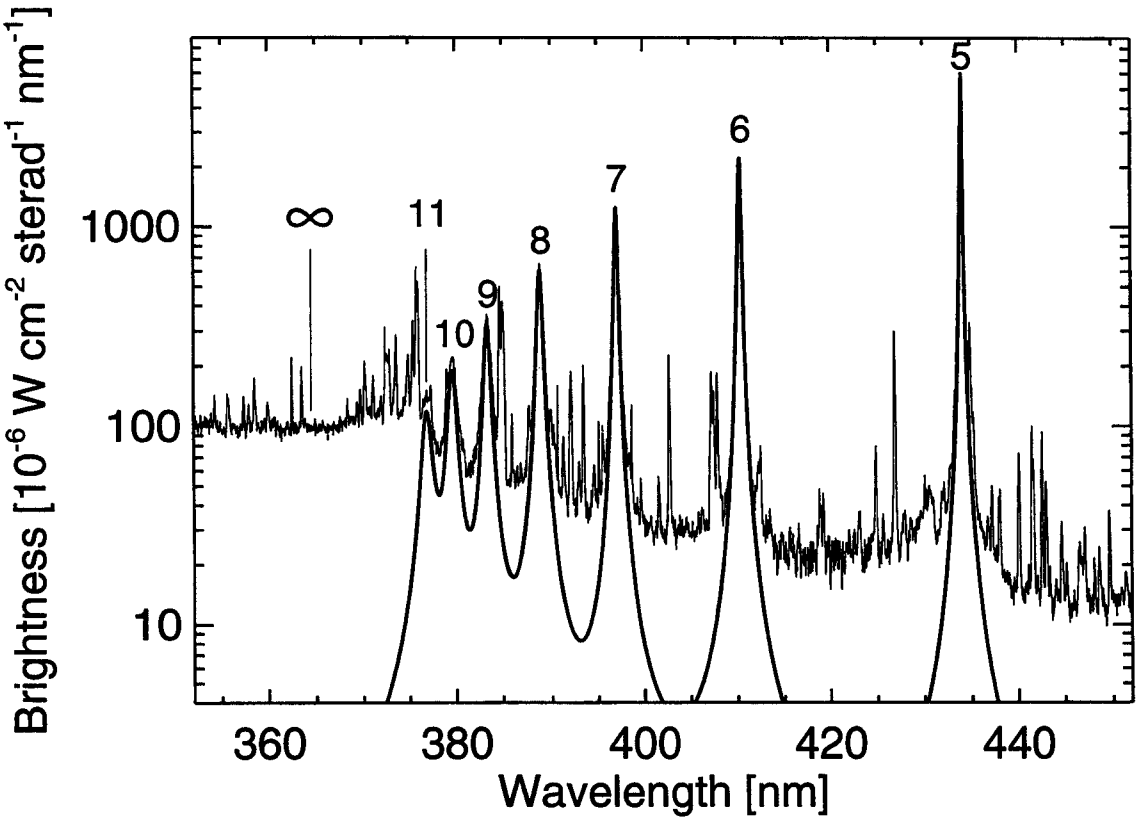

Figure 6: Fits to the measured Balmer series lines from upper states n=5 through n=11 are shown with the thick solid line. The line shapes are Lorentzian. The measured spectrum (Fig. 2) is also shown.

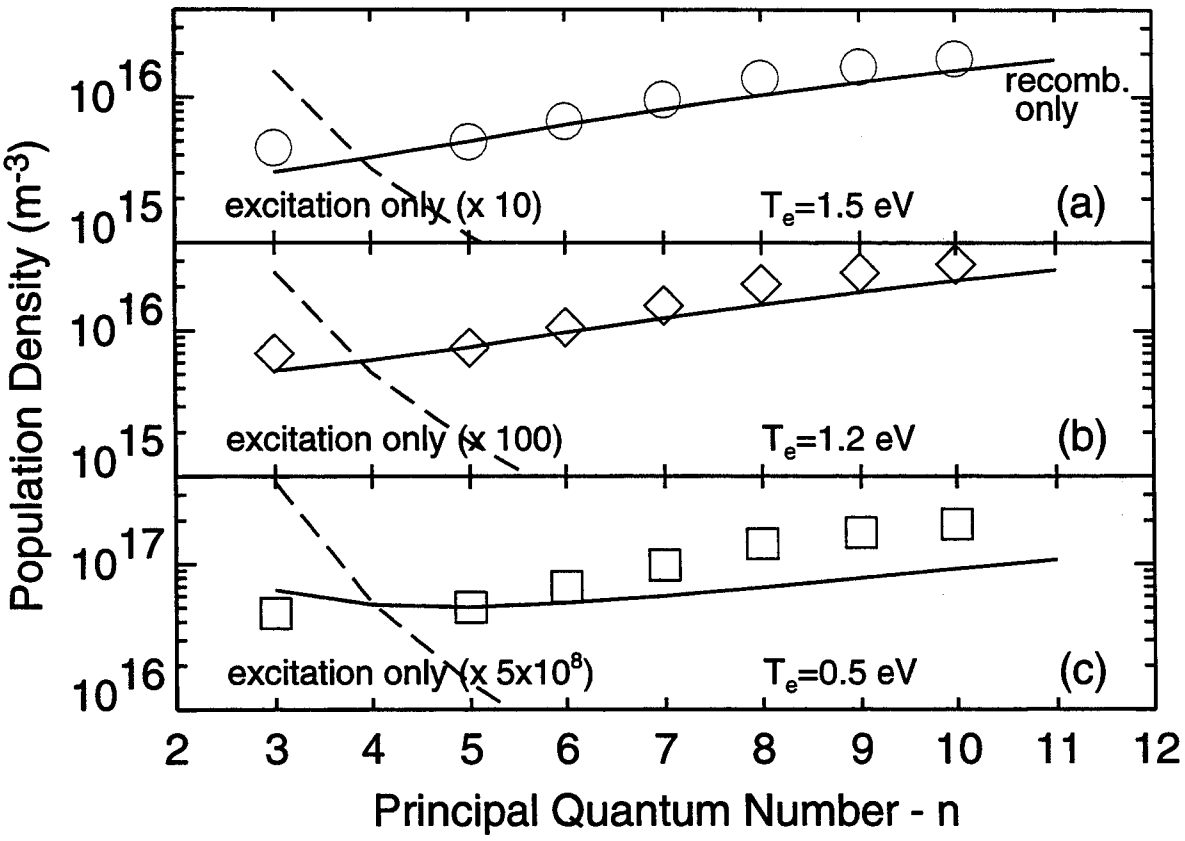

Figure 7: Comparison of the atomic level populations: The symbols represent the measured spectrum assuming: a) ΔL=0.051 m, b) ΔL=0.033 m, and c) ΔL=0.005 m. The theoretical predictions of the population densities resulting from recombination only are shown as solid lines. The predictions for population resulting from ground state excitation are shown with dashed lines. For the excitation contribution a ground state neutral density of 4×10^{20} m^{-3} has been assumed. The predictions are for three temperatures a) 1.5, b) 1.2 and c) 0.5 eV, each with $N_e = 8.8 \times 10^{20}$ m^{-3}.